RESEARCH PAPER

Criterion for flow liquefaction instability

José E. Andrade · Alfonso M. Ramos ·
Arcesio Lizcano

Abstract This study describes a general liquefaction flow instability criterion for elastoplastic soils based on the concept of loss of uniqueness. We apply the criterion to the general case of axisymmetric loading and invoke the concepts of effective stresses and loss of controllability to arrive at a general criterion for the onset of liquefaction flow. The criterion is used in conjunction with an elastoplastic model for sands to generate numerical simulations. The numerical results are compared with experimental evidence to give the following insights into predicting liquefaction. (1) The onset of liquefaction flow is a state of instability occurring under both monotonic and cyclic tests, and coincides with loss of controllability. (2) The criterion proposed herein clearly and naturally differentiates between liquefaction flow (instability) and cyclic mobility. (3) Flow liquefaction not only depends on the potential of the material to generate positive excess pore pressures, but more importantly, it also depends on the current state of the material, which is rarely predicted by phenomenology.

J. E. Andrade (✉)
Civil and Mechanical Engineering, California Institute
of Technology, 1200 E. California Blvd., Pasadena,
CA 91125, USA
e-mail: jandrade@caltech.edu

A. M. Ramos
Geophysical Institute, Pontificia Universidad Javeriana,
Cra 7 No 42-27, Bogotá, Colombia

A. Lizcano
SRK Consulting, 1066 West Hastings St.,
Vancouver V6E 3X2, Canada

List of symbols

A_0	Material constant in Dafalias Manzari model
A_d	Positive scaling function of dilatancy
c_h	Material constant in Dafalias Manzari model
d^2W	Second-order work per unit volume
e	Current void ratio
e_c	Void ratio on critical state line
e_0	Initial void ratio
e_{c0}	Critical state line material constant
F	Yield surface
G	Shear modulus
G_0	Elastic shear modulus
H	Hardening modulus
H_L	Critical hardening modulus
h	Positive state variable in Dafalias Manzari model
h_0	Material constant in Dafalias Manzari model
K	Bulk modulus
M	Critical stress ratio
m	Material constant in Dafalias Manzari model
M^b	Bounding stress ratio
M^d	Dilatancy stress ratio
n^b	Material constant in Dafalias Manzari model
n^d	Material constant in Dafalias Manzari model
η_{in}	Initial value of η at initiation of a new loading process
p	Volumetric stress
$\dot{p}$	Volumetric stress rate
P_{at}	Atmospheric pressure
Q	Plastic potential
q	Deviatoric stress
$\dot{q}$	Deviatoric stress rate
z	Fabric dilatancy factor
z_{max}	Material constant in Dafalias Manzari model
α	Back stress ratio
$\dot{\alpha}$	Evolution law for back stress

β	Dilatancy
$\dot{\epsilon}$	Strain vector increment
$\dot{\epsilon}_a$	Axial strain rate
$\dot{\epsilon}_r$	Radial strain rate
$\dot{\epsilon}_s$	Total deviatoric strain rate
$\dot{\epsilon}_s^e$	Elastic deviatoric strain rate
$\dot{\epsilon}_s^p$	Plastic deviatoric strain rate
$\dot{\epsilon}_v$	Total volumetric strain rate
$\dot{\epsilon}_v^e$	Elastic volumetric strain rate
$\dot{\epsilon}_v^p$	Plastic volumetric strain rate
η	Stress ratio
v	Poisson's ratio
ψ	State parameter
λ_c	Critical state line material constant
σ_a	Axial stress
σ_r	Radial stress
$\dot{\sigma}_a$	Axial stress rate
$\dot{\sigma}_r$	Radial stress rate
ξ	Critical state line material constant

1 Introduction

Liquefaction is one of the most elusive concepts in geotechnics due to its physical complexity and its relatively lax definition. Loosely defined, liquefaction can be associated with phenomena giving rise to loss of shearing resistance or the development of excessive strains, typically accompanied by increases in excess pore water pressures [24]. An alternative definition, typically used in mechanics, is that liquefaction is the phenomenon of vanishing inter-granular contact forces for some particular loading path [9]. More recently, the phenomenon has been divided into flow liquefaction and cyclic mobility [16, 24]. Flow liquefaction is associated with a state of instability and sudden increases in strain and pore pressures. It has been shown that flow liquefaction can be induced under monotonic or cyclic loading [6, 16, 17, 32]. This study provides a criterion for the onset of flow liquefaction instability. We treat flow liquefaction as an instability and make no distinction between monotonic and cyclic loads, thereby showing that this instability is a function of the state [2].

To date, there have been many attempts to detect the onset of flow liquefaction experimentally [1, 7, 13, 14, 27, 28, 30, 32, 34, 35]. On the theoretical side, different authors [12] have provided a criterion for loss of uniqueness that can be linked to a loss of stability in solids. Partly based on this criterion, works in [2, 4, 10, 11, 17, 23] and others have developed studies related to flow liquefaction, mostly for static liquefaction. In this study, besides deriving a general criterion for flow liquefaction, we begin to answer the following questions:

1. Is there a fundamental difference between liquefaction occurring under monotonic and cyclic loading?
2. Can analytical models differentiate between flow liquefaction and cyclic mobility?

In this work, we apply the notions of loss of uniqueness and loss of stability to a general class of isotropic elastoplastic models to apply a specific criterion for the onset of flow liquefaction. By choice, we make no distinction between so-called static liquefaction (e.g., [2]) and cyclic or dynamic liquefaction. The criterion is specialized to the context of classical 'triaxial' conditions applicable in the laboratory. The criterion is then adapted to a particular elastoplastic model capable of simulating cyclic and monotonic loading in sands [8]. We show that the resulting criterion is compatible with both the concept of loss of controllability [23] and the second-order work [10].

The paper is organized as follows. The first section of this study, Flow Liquefaction Criterion, shows the instability criterion using the concept of loss of uniqueness for a general family of isotropic elastoplastic constitutive models. The section 'Constitutive Model' presents the main features of the constitutive model used. The 'Numerical simulations' section presents three numerical simulations for prediction of flow liquefaction and compares them with laboratory experiments. Findings from the application of the criterion to each experiment are highlighted in the 'Conclusions' section.

2 Flow liquefaction criterion

For the sake of simplicity, and to validate our model against experimental data, we limit the following derivation to infinitesimal and axisymmetric undrained conditions. As shown before, loss of uniqueness requires [2, 3, 12]

$$[\![\dot{\boldsymbol{\sigma}}]\!] : [\![\dot{\boldsymbol{\epsilon}}]\!] = 0 \tag{1}$$

where $[\![\dot{\epsilon}]\!] = \dot{\epsilon}^* - \dot{\epsilon}$ is the jump in the strain rate due to potentially duplicate solutions ($\mathbf{v}^*$, $\mathbf{v}$) for the velocity field. Also, $[\![\dot{\boldsymbol{\sigma}}]\!]$ is the jump in the effective stress rate tensor, induced by the jump in the strain rate tensor. We note that the loss of uniqueness criterion begins with the total stress tensor but boils down to the expression above, given the undrained conditions imposed herein (see [2] for a complete argument). Now, under triaxial (axisymmetric) conditions, the above criterion reduces to

$$[\![\dot{p}]\!][\![\dot{\epsilon}_v]\!] + [\![\dot{q}]\!][\![\dot{\epsilon}_s]\!] = 0 \tag{2}$$

where $\dot{\epsilon}_v = \dot{\epsilon}_a + 2\dot{\epsilon}_r$ is the rate of volumetric strain and $\dot{\epsilon}_s = 2/3(\dot{\epsilon}_a + \dot{\epsilon}_r)$ is the deviatoric component of the strain rate. Also, $\dot{p} = 1/3(\dot{\sigma}_a + 2\dot{\sigma}_r)$ is the effective pressure rate

and $\dot{q} = \dot{\sigma}_a - \dot{\sigma}_r$ is the deviatoric stress rate. We note the usage of Cambridge $p-q$ stress invariants to describe triaxial conditions. Finally, $\dot{\sigma}_a$ is the axial total stress rate and $\dot{\sigma}_r$ is its radial counterpart.

Assuming a rate form for the constitutive relation, we typically write the relation between the effective stress rate and the total strain rate such that

$$\left\{\begin{array}{c} \dot{p} \\ \dot{q} \end{array}\right\} = \left[\begin{array}{cc} C_{pp} & C_{pq} \\ C_{qp} & C_{qq} \end{array}\right] \left\{\begin{array}{c} \dot{\epsilon}_v \\ \dot{\epsilon}_s \end{array}\right\} \tag{3}$$

where the constitutive matrix is furnished by the specific constitutive model of choice. Further, under undrained conditions, and assuming incompressible fluid and solid constituents, we require that $\dot{\epsilon}_v = 0$ and then use this fact together with Eqs. (2) and (3) to get that

$$C_{qq} [\![\dot{\epsilon}_s]\!]^2 = 0 \tag{4}$$

which implies in general that the shear component of the constitutive equation must vanish, i.e., $C_{qq} = 0$. This condition will furnish a general criterion for detecting flow liquefaction instability. We will adapt this general criterion to the case of the Manzari-Dafalias [8] constitutive model in the next section.

An interesting angle to observe is the similarity of this approach with the concepts of loss of controllability [23] and second-order work [10]. One can show that essentially Eq. (2) is the condition for nil second-order work. On the other hand, Nova [23] proposed the concept of loss of controllability under elemental test conditions. For instance, under undrained triaxial conditions, the volumetric strain rate and the deviatoric stress rates are controlled, given pressure increments and shear strain increments, such that.

$$\left\{\begin{array}{c} \dot{\epsilon}_v \\ \dot{q} \end{array}\right\} = \left[\begin{array}{cc} C_{pp}^{-1} & -C_{pq}C_{pp}^{-1} \\ C_{qp}C_{pp}^{-1} & C_{qq} - C_{pq}C_{qp}C_{pp}^{-1} \end{array}\right] \left\{\begin{array}{c} \dot{p} \\ \dot{\epsilon}_s \end{array}\right\} \tag{5}$$

Here, we look for the vanishing of the determinant of the matrix relating the controlled variables on the left to the emerging or responding variables on the right. The requirement of singularity implies $C_{qq}/C_{pp} = 0$ which, as before, requires

$$C_{qq} = 0 \tag{6}$$

Hence, the criterion presented herein, based on the concept of loss of uniqueness and imposing undrained conditions and effective stresses, coincides with the concept of second-order work and the concept of controllability. This establishes a necessary condition for flow liquefaction instability, and we will apply this criterion to a particular constitutive model in the next section. As it was already mentioned, the criterion is general in the sense that it applies to any elastoplastic

constitutive model of the form shown in Eq. (3). It rigorously applies to axisymmetric conditions of loading. Under conditions of different magnitude of stress in the three principal directions, the liquefaction criterion is only an approximation.

If one analyzes the mode of deformation as done by Nova [23], one can show that the corresponding increase in deviatoric strain is indefinite, accompanied by a corresponding increase in pore pressure. This is what Nova calls loss of controllability, which is identical to what we define here to be an instability: a large increase in response (e.g., pore pressures) due to a relatively small increase in excitation.

3 Constitutive model

Here, we briefly describe the Manzari-Dafalias [21] model with recent modifications [8] aimed at accounting for changes in fabric that might ultimately affect dilatancy. For a more complete description of the model, interested readers are referred to the original papers cited above. As shown in the literature, the Dafalias and Manzari constitutive model has been amply tested for simulating the behavior of granular soils subjected to monotonic and cyclic loading [15, 22, 29].

The constitutive model is framed in the critical state soil mechanics concept [26], and the elastic response is hypoelastic. The shear and bulk moduli are given such that

$$G = G_0 p_{at} \frac{(2.97 - e)^2}{1 + e} \left(\frac{p}{p_{at}}\right)^{1/2} \text{ and } K = \frac{2(1 + v)}{3(1 - 2v)} G \tag{7}$$

where G_0 is a constant, v is Poisson's ratio, e is the current void ratio, and p_{at} is the atmospheric pressure. The elastic region is enclosed by a yield surface in effective stress space which defines a wedge

$$F(\eta, \alpha) = |\eta - \alpha| - m \tag{8}$$

with $\eta = q/p$ as the stress ratio, α as the back stress, and m as a constant defining the width of the wedge so that in $p-q$ space, the wedge has an opening of $2mp$ at any value p. Figure 1 shows the geometrical attributes of the model in effective stress space. The inclination of the wedge defining the elastic region is given by the back stress whose evolution is governed by a kinematic hardening law

$$\dot{\alpha} = H\dot{\epsilon}_s^p \tag{9}$$

where H is the hardening modulus. To complete the description of the constitutive model, evolution of the hardening modulus H and dilatancy β must still be explained.

The hardening modulus is a function of the state of the material whose sign is controlled by its relative distance to the bounding stress, i.e.,
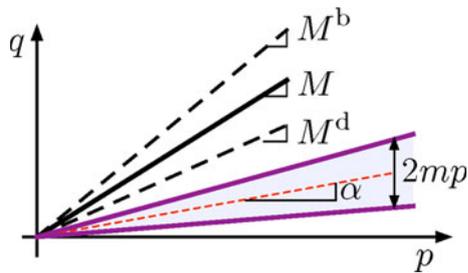
Fig. 1 Schematic of yield surface and main ingredients *plotted* in effective stress space. The *shaded area* represents the elastic region whose inclination is dictated by α. Other important ingredients are the bounding stress ratio M^b, dilatancy stress ratio M^d and the critical state ratio M

$$H = h(M^b - \eta) \quad \text{with} \quad h = \frac{G_0 h_0 (1 - c_h e)}{|\eta - \eta_{in}|} \left(\frac{p}{p_{at}}\right)^{-1/2} \quad (10)$$

where h is a positive function, M^b is the bounding stress ratio, and h_0 and c_h are positive constants. The evolution of the dilatancy β is given by a function similar to that of the hardening modulus, with the sign of the function dictated by its distance to the dilatancy stress so that

$$\beta = A_d (M^d - \eta) \quad (11)$$

with M^d as the dilatancy stress ratio, as shown in Fig. 1. While the value of η is less than the value of M^d, response is contractive. For all other cases, the model predicts dilation. The positive scaling function for dilatancy is affected by changes in fabric such that

$$A_d = A_0 (1 + \langle sz \rangle) \quad \text{with} \quad \dot{z} = -c_z \langle -\dot{\epsilon}_v^p \rangle (sz_{max} + z) \quad (12)$$

where A_0 is a positive constant and $s = \pm 1$ according to $\eta = \alpha \pm m$. The brackets $\langle \rangle$ are Macaulay brackets representing a ramp function. In addition, z_{max} represents the maximum possible value of the state parameter z.

The model is made to comply with critical state soil mechanics by postulating exponential evolution equations for the bounding and dilatancy stress ratios. They are respectively,

$$M^b = M \exp(-n^b \psi) \quad \text{and} \quad M^d = M \exp(n^d \psi) \quad (13)$$

with n^b and n^d as positive constants. Conceptually, the evolution equations shown above require M^b and M^d to coincide with M as $\psi \to 0$, requiring its state to tend to critical state. The state parameter $\psi = e - e_c$ was defined by Been and Jefferies [5] and measures the distance to the critical state from the current state in void ratio space. Finally, the critical state line is defined in void ratio space according to the relationship proposed by Li and Wang [20]

$$e_c = e_{c0} - \lambda_c (p_c/p_{at})^\xi \quad (14)$$

with e_{c0} as the void ratio at $p_c = 0$ and λ_c and ξ as constants.

The Dafalias and Manzari [8] constitutive model can be seen in the matrix form of Eq. (1) by re-sorting the additive decomposition of incremental stress–strain relation as follows

$$\dot{\epsilon}_s^e = \frac{\dot{q}}{3G} \quad \dot{\epsilon}_v^e = \frac{\dot{p}}{K} \quad (15)$$

$$\dot{\epsilon}_s^p = \frac{\dot{\eta}}{H} \quad \dot{\epsilon}_v^p = \beta |\dot{\epsilon}_s^p| \quad (16)$$

Superscripts e and p are the elastic and plastic part of strains. The increment in stress ratio is calculated as $\dot{\eta} = -\eta/p\dot{p} + \dot{q}/p$, where $\eta = q/p$. Based on the rates of total volumetric and deviatoric strains, Eq. (3) especially adapted to the Dafalias and Manzari [8] constitutive model reads

$$\begin{Bmatrix} \dot{p} \\ \dot{q} \end{Bmatrix} = \frac{1}{\chi} \begin{bmatrix} 3KG + KHp & -3KG\beta \text{sgn}(\dot{\epsilon}_s^p) \\ 3KG\eta & 3GHp - 3KG\beta\eta\text{sgn}(\dot{\epsilon}_s^p) \end{bmatrix} \begin{Bmatrix} \dot{\epsilon}_v \\ \dot{\epsilon}_s \end{Bmatrix} \quad (17)$$

where $\chi = 3G + Hp - K\beta\eta\text{sgn}(\dot{\epsilon}_s^p)$. Equation (6), which indicates loss of uniqueness and the onset of flow liquefaction, when especially adapted to the Dafalias and Manzari model is

$$C_{pp} = \frac{3G(Hp - K\beta\eta\text{sgn}(\dot{\epsilon}_s^p))}{\chi} = 0 \quad (18)$$

which, to be true in general, requires the quantity inside the parenthesis to vanish.

In elastoplastic models, the hardening modulus H is an indicator of the soil state. Andrade [2] deduced a critical hardening modulus as a predictor of static liquefaction for an elastoplastic constitutive model with two invariants. From Eq. (18), a closed form of the hardening modulus that is able to detect the onset of flow liquefaction can be proposed

$$H_L = \frac{K\beta\eta}{p} \text{sgn}(\dot{\epsilon}_s^p) \quad (19)$$

At the moment, when the hardening modulus equals the critical hardening modulus ($H - H_L = 0$), instability occurs in the form of flow liquefaction. It should be noted that for liquefaction instability to occur, undrained kinematic conditions have to be imposed and the liquefaction criterion $H - H_L = 0$ must be met. The instability criterion is a necessary buy not sufficient condition for liquefaction. This means that if $H - H_L$ is not zero, liquefaction cannot occur. On the other hand, if $H - H_L = 0$, then liquefaction may or may not occur.

Remark 1 The liquefaction criterion presented here is general to any elastoplastic model that can be cast in the

form given in Eq. (3). Since it is clear that the criterion is a function of the hardening modulus and the critical hardening modulus so that $H - H_L = 0$, we say that the criterion for liquefaction is a function of the state. The notion of state is rather general and dependent on the particular model used. We define state as the given stress, strain, and plastic internal variables affecting the 'state' of the material. The plastic internal variables could be many. In the particular model used here, these include void ratio and density, but other models could include other variables, for example fabric. The point is that since stress, strain, and plastic internal variables affect the hardening modulus and liquefaction criterion, we say that liquefaction here is defined as a function of the state. This is in sharp contrast with other criteria that define liquefaction as a material property [2].

In the following section, the criterion given by Eq. (19) will be evaluated by comparison against experimental laboratory tests available in the literature.

4 Numerical simulations

In this section, we present numerical simulations using the generalized flow liquefaction criterion introduced in Eq. (6) and adapted to the Manzari-Dafalias model utilizing the limiting hardening modulus encapsulated in Eq. (19). We compare these simulations with three different sets of experimental results where monotonic and cyclic stress paths were imposed for Toyoura sand, Nevada sand, and Dog's Bay sand, respectively. With exception of the parameters for the Toyoura sand, which were published by Dafalias and Manzari [8], the material parameters were calibrated based on the experiments which were simulated. Hence, simulations for the Toyoura sand experiments furnish a true prediction for the onset of liquefaction. The material parameters used in the model are shown in Table 1.

5 Verdugo and Ishihara [33] experiments on Toyoura sand

Verdugo and Ishihara [33] developed a series of monotonic undrained triaxial tests for a large range of initial compression pressures on Toyoura sand. Figure 2a shows the experiments with initial void ratio $e_0 = 0.833$ with mean pressure ranging from $p_0 = 100$ to $p_0 = 3,000$ kPa. The onset of flow liquefaction, marked by a star symbol in Fig. 2a, was obtained at the peak of deviatoric stress, and the instability line was built by joining the points marking the onset of flow liquefaction from each experiment. The

Table 1 Material parameters for the Manzari-Dafalias model for Toyoura, Nevada and Dog's Bay sand

Constant	Toyoura sand	Nevada sand	Dog's Bay sand
Elasticity			
G_0	125	125	140
v	0.05	0.05	0.05
Critical state			
M	1.25	1.45	1.55
λ_c	0.019	0.09	0.009
e_{c0}	0.934	0.737	1.015
ξ	0.7	1.0	0.5
Yield surface			
m	0.01	0.01	0.03
Plastic modulus			
h_0	7.05	4.5	7.05
c_h	0.968	1.05	0.968
n^b	1.1	1.1	1.1
Dilatancy			
A_0	0.704	0.804	0.5
n^d	3.5	5.5	3.5
Dilatancy-fabric			
z_{max}	4	10	40
c_z	600	500	2000

instability line is defined as the locus of points at which flow liquefaction is initiated for the same void ratio under undrained triaxial test [18, 31]. At this point, it is observed experimentally that axial strains and excess pore pressure increase significantly and suddenly. This is a direct result of the test being stress controlled. If the test is strain controlled, it can continue to impose increments in strain and no such loss of controllability is observed.

Parallel to the experimental results, we perform simulations on the Toyoura sand samples using the Dafalias and Manzari [8] model with parameters shown in Table 1. The same undrained boundary conditions are imposed and the effective stress paths obtained are plotted in Fig. 2b. The onset of flow liquefaction, as well as the instability line in the simulations (Fig. 2b), was detected by tracking the evolution of the critical hardening modulus and comparing it with the hardening modulus $H - H_L$. Figure 3 shows the evolution of the criterion of flow liquefaction for the simulations shown in Fig. 2b. It can be observed that only samples at 2,000 and 3,000 kPa confining pressures are able to liquefy. As observed in the experiments, the samples at lower confinement never reach the onset of liquefaction flow. In fact, the sample at 1,000 kPa confinement suffers a phase transition, as captured by the numerical simulation. These results clearly show that the criterion (and model) is able to distinguish between mechanical
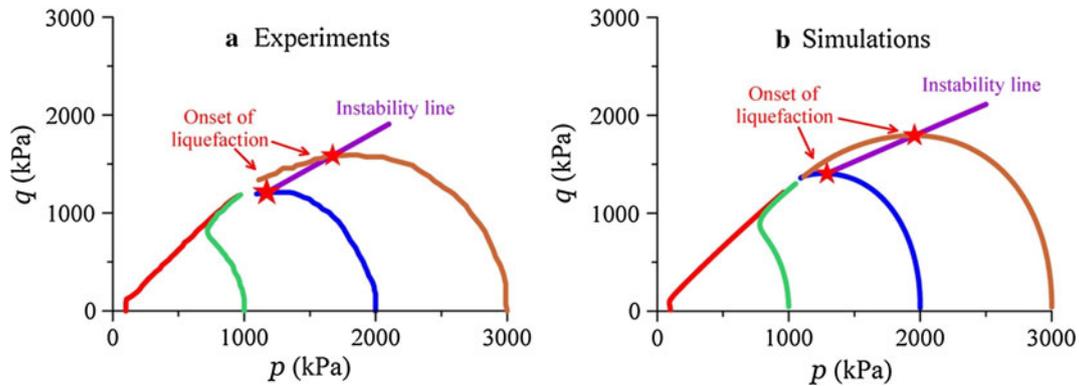
Fig. 2 **a** Experiments in undrained triaxial test for void ratio $e_0 = 0.833$ after Verdugo and Ishihara [33]. **b** Simulations of Verdugo and Ishihara tests
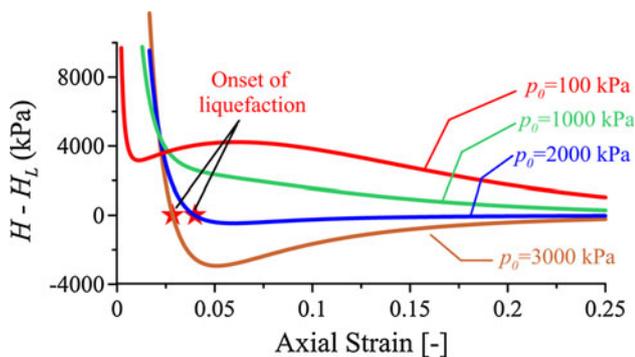
Fig. 3 Evolution of the flow liquefaction criterion compared to axial strains for simulations of undrained triaxial tests on Toyoura sands. Onset of flow liquefaction is marked at *points* where H equals H_L

behavior corresponding to denser than critical to that of sands that are looser than critical, or contractive. Contractive behavior is a necessary condition for flow liquefaction. Liquefaction is a function of the state.

6 Yamamuro and Covert [34] experiments on Nevada sand

Figure 4a depicts the undrained triaxial tests on Nevada sand performed by Yamamuro and Covert [34] for two initial confining pressures $p_0 = 200$ kPa and $p_0 = 350$ kPa with similar void ratios of $e_0 = 0.699$ and $e_0 = 0.711$, respectively. Both of these samples liquefied as indicated by the star symbol in Fig. 4a. Using the points demarking the onset of liquefaction, they obtained the instability line and compared it with the critical state line (CSL) or failure line. Figure 4b shows the numerical simulations of these monotonic tests, using the parameters reported in Table 1. The onset of flow liquefaction in the simulations was obtained by tracking the evolution of the critical hardening modulus H_L using Eq. (19), as illustrated before.

This data set is of particular interest because Yamamuro and Covert [34] looked at both monotonic and cyclic loading in Nevada sand at similar relative densities. This comparison is interesting as some of the phenomenology observed in monotonic tests is typically extrapolated to predict the onset of instabilities observed in cyclic tests. For example, the so-called instability line [19] is sometimes stretched out of context and used to predict the onset of instability when crossed during both monotonic and cyclic tests. Andrade [2] and others have shown that the instability line is a necessary but not sufficient condition for liquefaction flow. Hence, crossing the instability line does not guarantee liquefaction flow either in monotonic or cyclic tests. Another concept borrowed from monotonic test phenomenology is that of the so-called collapse boundary, which is interpreted as the locus defined by the corresponding effective stress path (e.g., Fig. 4a) for which flow liquefaction was observed during monotonic loading (see Sladen et al. [28] and Alarcón-Guzmán et al. [1]). It is believed that, for comparable states, when the effective stress path during cyclic loading has crossed the instability line and intercepts the collapse surface, the samples display flow liquefaction instability. The above two criteria are typically used to predict the onset of flow liquefaction instability.

Figure 5a shows a cyclic triaxial compression test developed by Yamamuro and Covert [34]. The sample was isotropically compressed at $p_0 = 225$ kPa, followed by anisotropic compression until $p = 250$ and $q = 75$ kPa. At this stage, an undrained cyclic triaxial test was performed with a controlled stress amplitude of $\Delta q = 46$ kPa and an initial void ratio of $e_0 = 0.712$. Also, Fig. 5a shows the instability line and the undrained monotonic triaxial test for $e_0 = 0.711$ of Fig. 4a. The monotonic stress path could be considered to be the collapse boundary for the cyclic triaxial tests. Indeed, it is observed that the sample under cyclic loading reaches flow liquefaction very close to the
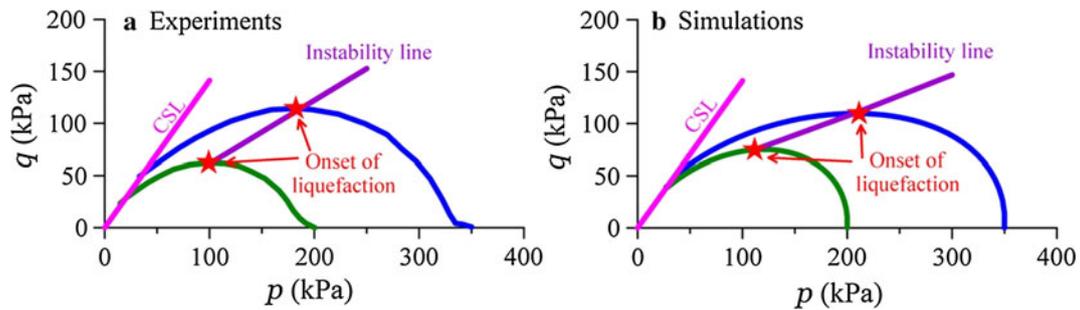
Fig. 4 **a** Undrained triaxial tests of Yamamuro and Covert [34]. $P_0 = 200$ kPa $e_0 = 0.699$ and $P_0 = 350$ kPa $e_0 = 0.711$. **b** Simulations of Yamamuro and Covert tests

collapse boundary. However, this is an extrapolation, and 'proximity' to the collapse boundary varies. The liquefaction flow criterion presented herein does not need to assume any phenomenology a priori to detect the onset of instability.

Figure 5b shows the results corresponding to the cyclic test shown in Fig. 5a. As before, this simulation is run using the parameters in Table 1, and the onset of instability is obtained by tracking the liquefaction criterion as reported in Fig. 6. From Fig. 6, it is evident that the liquefaction criterion $H - H_L$ is not continuous. This is due to the elastic unloading experienced as the samples switch from compression to extension. Naturally, the hardening modulus, and hence the liquefaction criterion, is only defined during plastic loading. Superimposed on Fig. 5b is the monotonic effective stress path from Fig. 4b, which furnish a collapse boundary. As in the experimental result, the onset of liquefaction flow during cyclic loading is obtained after crossing the instability line and close to the collapse boundary. However, neither the instability line nor the collapse boundary serve as predictors for flow liquefaction. On the other hand, the criterion presented here did not need to borrow from phenomenology and it is able to detect the onset of flow liquefaction during both monotonic and cyclic loading. This demonstrates that loss of controllability [23] is obtained during monotonic and cyclic tests and that instability in both cases is a function of the state.
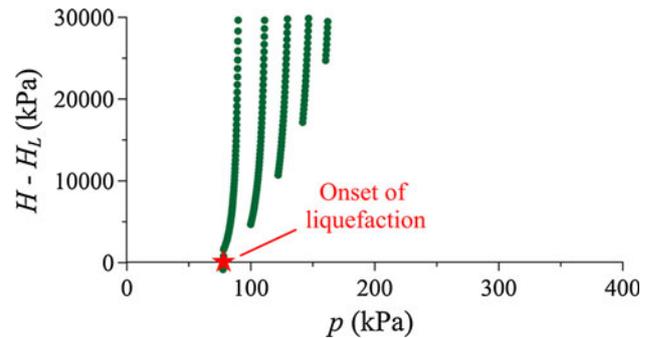
Fig. 6 Evolution of $H - H_L$ for the cyclic triaxial test of the simulation in Fig. 5b. Onset of flow liquefaction under cyclic loading conditions is marked by a *star*

7 Qadimi and Coop [25] experiments on Dog's bay sand

Figure 7a depicts an undrained cyclic triaxial test performed by Qadimi and Coop [25] using Dog's Bay sand. It is anisotropically consolidated under a K_0 stress path. The initial state of stresses before the undrained cyclic test was $q = 1,828$ and $p = 2,500$ kPa. The void ratio before the cyclic test was $e_0 = 0.982$. The increment of deviatoric stress for the undrained cyclic triaxial test was $\Delta q = 1,000$ kPa. As shown in Fig. 7a, after a couple tens of cycles, the specimen displayed liquefaction flow with a
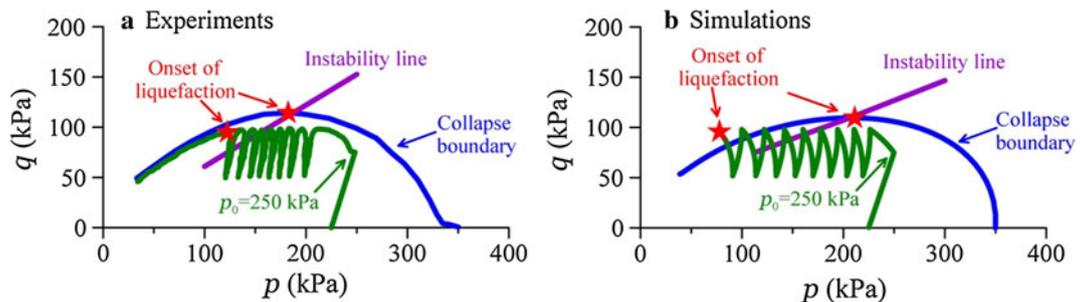
Fig. 5 **a** Experimental monotonic and cyclic triaxial tests developed by Yamamuro and Covert [34] $e \approx 0.7$. **b** Simulations of monotonic and cyclic triaxial tests developed by Yamamuro and Covert [34] $e \approx 0.7$

sudden increase in pore water pressure as evidenced by the remarkable drop in effective pressure and the loss of controllability (also see Fig. 10). This set of experiments is particularly interesting because it helps illustrate the difference between flow liquefaction and cyclic mobility.

Parallel to the anisotropically consolidated test, we performed a simulation with parameters specified in Table 1. The effective stress path of the corresponding simulation is shown in Fig. 7b. Similar to the actual experiment, flow liquefaction is detected after 19 cycles. As before, detection of flow liquefaction is signaled by $H - H_L = 0$, as shown in Fig. 8. The simulation reproduces faithfully the stress path and the onset of liquefaction. Similar to the results obtained for the Yamamuro and Covert [34] test, the current simulations display a loss of controllability when the liquefaction criterion is met, manifesting in an inability to further impose the prescribed deviatoric stress increment Δq. At the onset of liquefaction, the sample is very close to a phase transformation, but this is never fully realized, as the sample never has the chance to experience hardening because liquefaction and the associated loss of controllability occur just before.

Similar to the anisotropically consolidated test shown above, Qadimi and Coop [25] performed an undrained cyclic test after isotropic consolidation. The void ratio for this test was very similar to the above with $e_0 = 1.22$. Hence, these two tests provide a backdrop to evaluate the differences between liquefaction flow and cyclic mobility. Figure 9a shows a simulation of an undrained cyclic triaxial test isotropically compressed at $p_0 = 1{,}400$ kPa as performed by Qadimi and Coop [25]. The prescribed increment of cyclic deviatoric stress is $\Delta q = 280$ kPa. One hundred and fifty (150) cycles of deviatoric stress were applied. Figure 9b shows the evolution of the criterion for flow liquefaction ($H - H_L$) for the numerical experiment
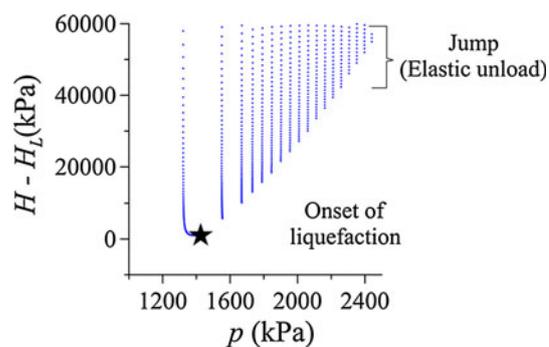
Fig. 8 Evolution of $H - H_L$ for the simulation of the anisotropically consolidated undrained cyclic triaxial test performed by Qadimi and Coop [25]

shown in Fig. 9a. Although there is a decrease in effective mean pressure as a result of cyclic loading, the criterion for liquefaction flow is never satisfied after 150 cycles. This behavior is similar to that observed in the experiments where cyclic mobility was observed, as opposed to liquefaction flow.

The buildup of pore pressure generated in the two previous undrained cyclic triaxial tests (Figs. 7a and 9a) was reported by Qadimi and Coop [25] and is redrawn in Fig. 10. The buildup of pore pressure obtained in the simulations is superimposed on the figure. Excess pore water pressures, normalized by the mean pressure after consolidation, are plotted in Fig. 10 as a function of the number of cycles. It can be seen that the buildup of pore water pressures is significantly different for the anisotropically consolidated sample relative to the isotropically consolidated counterpart. There is a sharp increase in pore pressures after a few tens of cycles in the anisotropic sample. This is characteristic of liquefaction flow. On the other hand, as it is characteristic of cyclic mobility, the
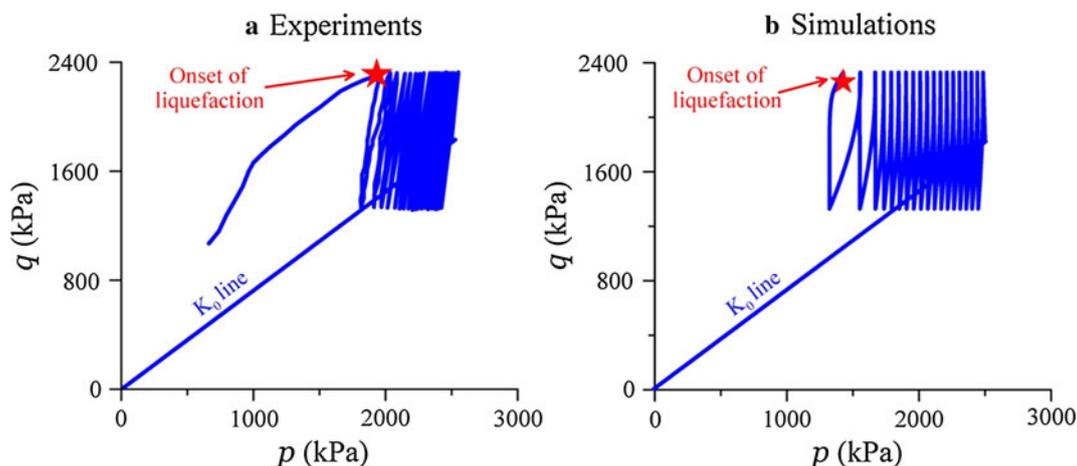
Fig. 7 **a** Experimental undrained cyclic triaxial test anisotropically consolidated with a K_0 condition of $e_0 = 0.982$, $\Delta q = 1000$ kPa by Qadimi and Coop [25]. **b** Simulation of Qadimi and Coop [25] test
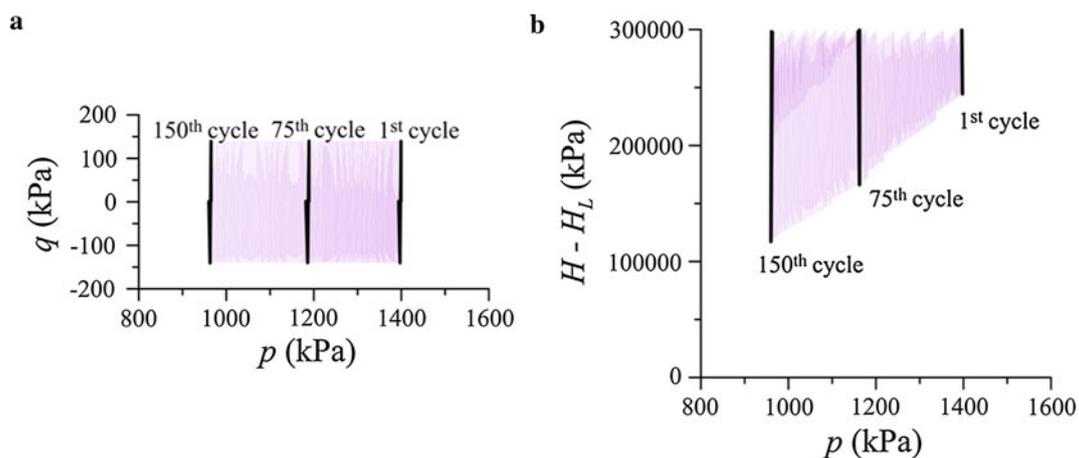
Fig. 9 **a** Simulation of an undrained cyclic triaxial test isotropically compressed at $p_0 = 1,400$ kPa in Dog′s Bay sand. Initial void ratio $e_0 = 1.22$. Increment of deviatoric cyclic stress $\Delta q = 280$ kPa at 150 loading cycles. **b** Evolution of the criterion for flow liquefaction for simulation shown in Fig. 9a

isotropically consolidated sample displays a smooth increase in pore pressures, without noticeable sudden changes. In fact, as seen in Fig. 10, after 150 cycles, the sample has reached about 50 % of the normalized pore pressure increase experienced by the anisotropic sample. This is emblematic of the mechanical difference between liquefaction flow and cyclic mobility. As anticipated by Alarcón-Guzmán et al. [1], flow liquefaction is an insta-bility obtained as part of structural collapse in a sample of sand. It typically displays sudden increases in strains and excess pore pressure. On the other hand, cyclic mobility is a constitutive response, with accumulation of strains and excess pore pressures without exhibiting measurable instabilities. We have shown that the liquefaction criterion presented herein is able to distinguish between flow liq-uefaction and cyclic mobility.
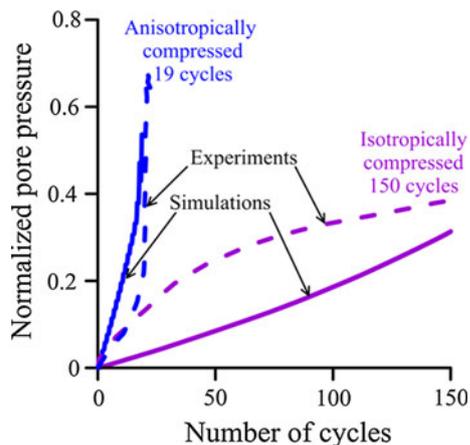
Fig. 10 Buildup of excess pore pressure for the cyclic experiments depicted in Figs. 7a, 9a *plotted* against number of cycles. Experiments were performed by Qadimi and Coop [25]

Remark 2 Both experiments and simulations are per-formed under undrained kinematic conditions (constant volume here) and prescribed changes in stress deviator. The experiments which attain flow liquefaction seem to be able to progress, but, if one observes, they have lost con-trollability (i.e., the prescribed cycles of change in stress deviator cannot be completed as specified). On the other hand, the numerical simulations cannot continue at the point of liquefaction, loose controllability, and crash.

Remark 3 One can observe from Fig. 9 (especially b) that if the trend is continued, even after 200 cycles, simulations remain stable and variations in deviator stress can still be controlled. Now, what happens with the increase in pore pressure is completely dependent on the dilatancy evolu-tion, which is a feature of the plasticity model. The model could be evolving dilatancy inaccurately. The main points made by Figs. 7, 8, 9, 10 are (1) the simulations can cap-ture the main features of the experiments, (2) show that the model can detect liquefaction instability when it occurs, and (3) show that liquefaction is an instability, whereas cyclic mobility is not. Instability is never observed in the isotropically consolidated sample, which simply reaches critical state and displays the so-called butterfly effect, never loosing controllability. Whereas the anisotropic sample looses controllability after only 19 cycles, dis-playing a sudden increase in pore pressures.

Remark 4 While no conclusive statements can be made based on one example to differentiate flow liquefaction and cyclic mobility, it is clear that this example shows vast differences in the mechanism, with flow liquefaction being associated with an unstable state. On the other hand, cyclic mobility is an incremental state and does not display unstable effects. This last statement is not new (e.g., [16]), but the results shown in this study give a clear mechanics

framework to differentiate between flow liquefaction and cyclic mobility.

8 Conclusions

We have presented a general criterion for detecting the onset of flow liquefaction and have applied it to a particular elastoplastic constitutive model for sands capable of simulating the behavior of the material under monotonic and cyclic tests. We have used three different sets of data to illustrate the predictive capabilities of the proposed criterion.

Based on the results obtained in this study, we reach the following conclusions:

- The liquefaction criterion presented herein can detect the onset of liquefaction flow under both monotonic and cyclic conditions without resorting to assumptions a priori.
- Flow liquefaction, as detected by the criterion presented in Eq. (6), corresponds to a collapse or instability, which is a function of the state of the material.
- As observed in experiments, both cyclic mobility and flow liquefaction display increases in pore pressures, with cyclic mobility producing gradual pore pressure buildup and flow liquefaction producing sudden pore pressure buildup as a result of material instability. The criterion presented herein captures this difference as a natural result of the state of the material.
- The instability line and the collapse boundary are necessary conditions for instability but are certainly not sufficient or predictive.
- The $H - H_L$ could help predict the liquefaction potential for a given soil based on its state and imposed loading path.

References

1. Alarcón-Guzmán A, Leonards A, Chameau L (1988) Undrained monotonic and cyclic strength of sands. J Geotech Eng 114(10): 1089–1108
2. Andrade JE (2009) A predictive framework for liquefaction instability. Géotechnique 59(8):673–682
3. Borja RI (2002) Bifurcation of elastoplastic solids to shear band mode at finite strains. Comput Methods Appl Mech Eng 191(46): 5287–5314
4. Borja RI (2006) Condition for liquefaction instability in fluid-saturated granular soils. Acta Geotech 1(4):211–224
5. Been K, Jefferies MG (1985) A state parameter for sands. Géotechnique 35:99–112
6. Castro G (1969). Liquefaction of sands, Harvard Soil Mechanics Series, No.81, Pierce Hall
7. Castro G (1987). On the behaviour of soils during earthquake liquefaction. Technical report, Geotechnical engineers Inc., Winchester, MA. 01890. USA
8. Dafalias YF, Manzari MT (2004) Simple plasticity sand model accounting for fabric change effects. J Eng Mech 130(6):622–633
9. Darve F (1996) Liquefaction phenomenon of granular materials and constitutive instability. Eng Comput 13(7):5–28
10. Darve F, Laouafa F (2000) Instabilities in granular materials and application to landslides. Mech Cohesive-Frictional Mater 5(8): 627–652
11. Gajo A (2004) The influence of system compliance on collapse of triaxial sand samples. Can Geotech J 41:257–273
12. Hill R (1958) A general theory of uniqueness and stability in elastic-plastic solids. J Mech Phys Solids 6(3):236–249
13. Hyde A, Higuchi T, Yasuhara K (2006) Liquefaction, cyclic mobility, and failure of silt. J Geotech Geoenviron Eng 132(6):716–731
14. Ishihara K, Tatsuoka F, Yasuda S (1975) Undrained deformation and liquefaction of sand under cyclic stress. Soils Found 15(1): 29–44
15. Jeremic B, Cheng Z, Taiebat M, Dafalias Y (2008) Numerical simulation of fully saturated porous material. Int J Numer Anal Meth Eng 24:1636–1660
16. Kramer SL (1996) Geotechnical earthquake engineering. Prentice Hall International Series, New Jersey
17. Lade PV (1992) Static instability and liquefaction of loose fine sandy slopes. J Geotech Eng 118:51–71
18. Lade PV (1994) Instability and liquefaction of granular materials. Comput Geotech 16(2):123–151
19. Lade PV (1999) Instability of granular materials. In: Lade PV, Yamamuro JA (eds) Physics and mechanics of soil liquefaction. Balkema, Rotterdam, pp 3–16
20. Li XS, Wang Y (1998) Linear representation of steady-state line for sand. J Geotech Geoenviron Eng 124(12):1215–1217
21. Manzari MT, Dafalias YF (1997) A critical state two-surface plasticity model for sands. Géotechnique 47(2):255–272
22. Manzari MT, Prachathananukit R (2001) On integration of a cyclic soil plasticity model. Int J Numer Anal Meth Geomech 25:525–549
23. Nova R (1994) Controllability of the incremental response of soil specimens subjected to arbitrary loading programmes. J Mech Behav Mater 5:193–201
24. National Research Council (NRC) (1985) Liquefaction of soils during earthquakes. National Academy Press, Washington DC
25. Qadimi A, Coop M (2007) The undrained cyclic behaviour of a carbonate sand. Géotechnique 57(9):739–750
26. Schofield A, Wroth P (1968) Critical state soil mechanics. McGraw-Hill, New York
27. Seed H (1979). Soil liquefaction and cyclic mobility evaluation for level ground during earthquakes. J Geotech Eng Division 105 (GT2) pp 201–255
28. Sladen J, D'hollander R, Hight D (1985) The liquefaction of sands, a collapse surface approach. Can Geotech J 22(4):564–578
29. Taiebat M, Jeremic B, Dafalias Y, Kaynia A, Cheng Z (2010) Propagation of seismic waves through liquefied soils. Soils Dyn Earthquake Eng 30:236–257
30. Vaid YP, Chern JC (1983) Effect of static shear on resistance to liquefaction. Soils Found 23:47–60
31. Vaid YP, Chern JC (1985) Cyclic and monotonic undrained response of saturated sand. Advances in the Art of Testing Soils under Cyclic Conditions. ASCE, pp 120–147

32. Vaid YP, Sivathalayan S (2000) Fundamental factors affecting liquefaction susceptibility of sands. Can Geotech J 37(3):592–606
33. Verdugo R, Ishihara K (1996) The steady state of sandy soils. Soils Found 33:81–92
34. Yamamuro J, Covert K (2001) Monotonic and cyclic liquefaction of very loose sands with high silt content. J Geotech Geoenviron Eng 127(4):314–324
35. Yilmaz Y, Mollamahmutoglu M (2009) Characterization of liquefaction susceptibility of sands by means of extreme void ratios and/or void ratio range. J Geotech Geoenviron Eng 135(12): 1986–1990